BIOLOGICAL CRYSTALLOGRAPHY

ISSN 1399-0047

Structure of the RsbX phosphatase involved in the general stress response of *Bacillus subtilis*

Aik-Hong Teh,[a,b]‡ Masatomo Makino,[a,c]‡ Takeshi Hoshino,[a] Seiki Baba,[a] Nobutaka Shimizu,[a] Masaki Yamamoto[d] and Takashi Kumasaka[a]*

[a]Japan Synchrotron Radiation Research Institute (JASRI/SPring-8), 1-1-1 Kouto, Sayo, Hyogo 679-5198, Japan, [b]Centre for Chemical Biology, Universiti Sains Malaysia, Penang 11900, Malaysia, [c]Shimane Institute for Industrial Technology, 1 Hokuryo-cho, Matsue, Shimane 690-0816, Japan, and [d]RIKEN SPring-8 Center, 1-1-1 Kouto, Sayo, Hyogo 679-5148, Japan. *Correspondence e-mail: kumasaka@spring8.or.jp

Received 3 December 2014
Accepted 9 April 2015

Edited by Z. S. Derewenda, University of Virginia, USA

‡ These authors contributed equally to this work.

Keywords: signalling protein; stressosome; environmental stress; dephosphorylation; protein phosphatase; manganese binding.

PDB references: RsbX, complex with cobalt, space group *P*1, 3w45; complex with magnesium, space group *P*1, 3w40; space group $P2_1$, 3w41; complex with manganese, space group *P*1, 3w42; space group $P2_1$, 3w43; selenomethionine derivative, 3w44

Supporting information: this article has supporting information at journals.iucr.org/d

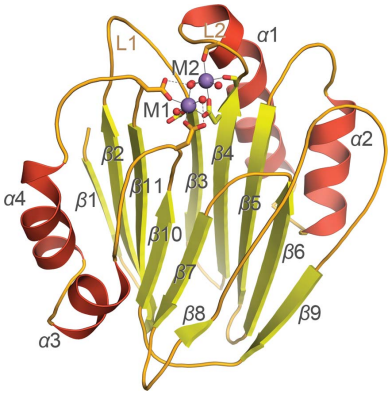

In the general stress response of *Bacillus subtilis*, which is governed by the sigma factor σ^B, stress signalling is relayed by a cascade of Rsb proteins that regulate σ^B activity. RsbX, a PPM II phosphatase, halts the response by dephosphorylating the stressosome composed of RsbR and RsbS. The crystal structure of RsbX reveals a reorganization of the catalytic centre, with the second Mn^{2+} ion uniquely coordinated by Gly47 O from the $\beta4$–$\alpha1$ loop instead of a water molecule as in PPM I phosphatases. An extra helical turn of $\alpha1$ tilts the loop towards the metal-binding site, and the $\beta2$–$\beta3$ loop swings outwards to accommodate this tilting. The residues critical for this defining feature of the PPM II phosphatases are highly conserved. Formation of the catalytic centre is metal-specific, as crystallization with Mg^{2+} ions resulted in a shift of the $\beta4$–$\alpha1$ loop that led to loss of the second ion. RsbX also lacks the flap subdomain characteristic of PPM I phosphatases. On the basis of a stressosome model, the activity of RsbX towards RsbR-P and RsbS-P may be influenced by the different accessibilities of their phosphorylation sites.

1. Introduction

Bacteria possess a general stress-response mechanism that allows them to react swiftly towards a wide range of environmental and energy stresses. In *Bacillus subtilis*, these stress signals are relayed by a signalling cascade that ultimately activates the alternative sigma factor σ^B, leading to the expression of general stress proteins (Haldenwang, 1995; Hecker & Völker, 1998; Price *et al.*, 2001). The cascade consists of three modules made up of nine Rsb (regulators of σ^B) proteins: one directly regulates σ^B activity (RsbV and RsbW; Dufour & Haldenwang, 1994; Delumeau *et al.*, 2002), while the other two relay either the environmental (RsbR, RsbS, RsbT, RsbU and RsbX; Dufour *et al.*, 1996; Yang *et al.*, 1996) or energy stress signals (RsbP and RsbQ; Vijay *et al.*, 2000; Brody *et al.*, 2001) to the first module. Signal transduction utilizes reversible phosphorylation–dephosphorylation and partner switching of the component proteins. In the environmental stress-response pathway, RsbR and RsbS form a gigantic stressosome through their STAS (sulfate transporter and anti-σ factor antagonist) domains, capturing RsbT in the absence of stress (Chen *et al.*, 2003; Marles-Wright *et al.*, 2008). Exposure to stress triggers the phosphorylation of RsbR and RsbS by the kinase RsbT, resulting in the release of RsbT from the stressosome and the subsequent activation of RsbU by RsbT (Kim *et al.*, 2004; Chen *et al.*, 2004), finally leading to σ^B activation.

RsbX is a phosphatase that dephosphorylates both RsbR-P and RsbS-P, reinstating the stressosome to its steady state that

recaptures RsbT (Yang *et al.*, 1996; Chen *et al.*, 2004). This resetting is important, as null mutations in the *rsbX* gene inhibited cell growth because of high σ^B activity (Igo *et al.*, 1987; Benson & Haldenwang, 1992). The environmental and energy stress modules each also contain another phosphatase, RsbU or RsbP, which acts on phosphorylated RsbV (Yang *et al.*, 1996; Vijay *et al.*, 2000). All three of the phosphatases RsbX, RsbU and RsbP belong to subfamily II (PPM II) of the Ser/Thr phosphatase PPM family (Bork *et al.*, 1996; Shi, 2004). PPM phosphatases are composed of a PP2C core that binds two divalent metal ions, either Mg^{2+} or Mn^{2+}, in the catalytic centre, and are involved in a wide range of cellular processes. The PPM mechanism was first described in human PP2Cα from subfamily I (PPM I), which regulates the mitogen-activated protein kinase pathway (Das *et al.*, 1996; Takekawa *et al.*, 1998), and was fine-tuned further when a new structure with a phosphate ion bound directly to the two metal ions was obtained for MspP, a PPM I phosphatase from the saprophyte *Mycobacterium smegmatis* (Bellinzoni *et al.*, 2007). PPM II phosphatases lack motifs that constitute a highly variable flap found in PPM I phosphatases (Shi, 2004). This flap is observed to bind a third metal ion in several structures (Pullen *et al.*, 2004; Bellinzoni *et al.*, 2007; Schlicker *et al.*, 2008; Rantanen *et al.*, 2007), although in some phosphatases this ion is not necessary for their activity towards the nonspecific phosphatase substrate *p*-nitrophenylphosphate (*p*NPP; Schlicker *et al.*, 2008; Wehenkel *et al.*, 2007).

While RsbU and RsbP contain additional N-terminal domains, RsbX consists of only a single phosphatase domain. At present several PPM II phosphatase structures are known, including MtX, Rv1364c and SpoIIE. MtX is an RsbX orthologue from *Moorella thermoacetica*, which also forms a similar stressosome that regulates the biosynthesis of the secondary messenger signalling molecule cyclic di-GMP (Quin *et al.*, 2012). Rv1364c from *M. tuberculosis*, meanwhile, is a multidomain regulatory protein containing a PAS and phosphatase domain, a kinase domain and a STAS domain that resemble RsbP, RsbW and RsbV, respectively (King-Scott *et al.*, 2011). SpoIIE, on the other hand, is involved in the sporulation of *B. subtilis* and dephosphorylates SpoIIAA-P to trigger the activation of σ^F (Duncan *et al.*, 1995; Levdikov *et al.*, 2012). We have solved the structure of RsbX in six crystal forms that bind either one or two metal ions. These PPM I structures feature a catalytic centre with a highly conserved loop that coordinates the second metal ion, which is not observed in PPM I phosphatases. In the RsbX structures, the accompanying conformational changes in the loop region further show that formation of the catalytic centre is metal-specific.

2. Materials and methods

2.1. Protein expression and purificaiton

Wild-type RsbX was prepared as described previously (Suganuma *et al.*, 2009), while selenomethionine (SeMet)-labelled RsbX was expressed in cells grown in SeMet core medium (Wako, Japan) supplemented with 10 g l^{-1} glucose, 250 mg l^{-1} $MgSO_4{\cdot}7H_2O$, 4.18 mg l^{-1} $FeSO_4{\cdot}7H_2O$, 0.5 mg l^{-1} thiamine, 50 mg l^{-1} DL-selenomethionine and 50 mg l^{-1} ampicillin. Briefly, the cells were grown either in LB or SeMet core medium at 37°C and protein expression was induced with 1 m*M* IPTG when the cell culture reached an OD_{600} of 0.7. After overnight incubation at 18°C, the cells were harvested, lysed by sonication in 50 m*M* Tris–HCl, 0.5 *M* NaCl, 1 m*M* dithiothreitol pH 8.0 and centrifuged. The supernatant was loaded onto a chitin-affinity column (NEB) at 4°C and self-cleavage of the tag was initiated with 70 m*M* DTT for 48 h. The eluted protein was further gel-filtrated on Superdex 75 (GE Healthcare) in 50 m*M* Tris–HCl, 0.2 *M* NaCl, 1 m*M* DTT pH 8.0.

2.2. Phosphatase assays with *p*NPP

Enzymatic assays were performed with the substrate *p*NPP, the hydrolysis product of which, *p*-nitrophosphate, was detected by measuring the absorbance at 405 nm with a 96-well GENios microplate reader (Tecan). Each measurement was performed at least in triplicate, and the values of k_{cat} and K_m were estimated by fitting the data to the Michaelis–Menten equation. For determination of the *p*NPP kinetic constants, RsbX was incubated with a reaction buffer consisting of 50 m*M* Tris pH 8.0, 1 m*M* TCEP, 5 m*M* $MnCl_2$, 0.5–5.0 m*M* *p*NPP. The Mn^{2+} kinetic constants, meanwhile, were determined in 10 m*M* *p*NPP, 0.2–2.0 m*M* $MnCl_2$. For the metal-dependence assays, $MnCl_2$ was replaced by $MgCl_2$, $CoCl_2$, $NiCl_2$, $CuCl_2$ or $ZnCl_2$.

2.3. Crystallization and data collection

As previously described (Suganuma *et al.*, 2009), RsbX was crystallized at 20°C in 20% PEG 1000, 0.1 *M* Tris–HCl pH 8.5, 5 m*M* $MgCl_2$. $MgCl_2$ was substituted by $MnCl_2$, $CoCl_2$, $NiCl_2$, $CuCl_2$ or $ZnCl_2$ in order to utilize their anomalous signals for phasing, but no crystals were formed. Only when streak-seeding with the Mg^{2+}-derived crystals in the initial crystallization buffer supplemented with 1–3 m*M* $MnCl_2$, $CoCl_2$ or $NiCl_2$ was performed did crystals begin to form. Streak-seeding with Mn^{2+} produced fewer but larger crystals than with Mg^{2+}. Diffraction data were successfully collected at 100 K on beamline BL41XU at SPring-8 for RsbX co-crystallized with Mg^{2+} (Mg_1-*A*), Mn^{2+} (Mn_1) or Co^{2+} (Co_1). After integration and scaling with *HKL*-2000 (Otwinowski & Minor, 1997), all of the crystals were found to belong to the same space group, *P*1, with similar unit-cell parameters and with two molecules in the asymmetric unit related by 2_1 symmetry. A second crystal form, belonging to space group $P2_1$ (Mg_1-*B*), was obtained for the Mg^{2+} crystals after repeated annealing.

Subsequent optimization trials also yielded crystals in 25% PEG 1000, 0.1 *M* Tris–HCl pH 8.5, 10 m*M* $MnCl_2$, and data collection on beamline BL38B1 at SPring-8 revealed another crystal form in space group $P2_1$ (Mn_2). Crystals of selenomethionine-labelled RsbX formed in 27% PEG 4000, 90 m*M* Tris–HCl pH 8.5, 0.18 *M* $MgCl_2$, 0.12 *M* $MnCl_2$, and diffraction

Table 1
Data-collection and refinement statistics for RsbX crystals.

Values in parentheses are for the outer shell.

Crystal	Mn_2	Mn_2-Se	Mn_1	Mg_1-*A*	Mg_1-*B*	Co_1
Bound ion	2 Mn^{2+}	2 Mn^{2+}	1 Mn^{2+}	1 Mg^{2+}	1 Mg^{2+}	1 Co^{2+}
Wavelength (Å)	1.0000	0.9780	1.0000	1.0000	1.0000	1.6047
Space group	$P2_1$	$P4_222$	$P1$	$P1$	$P2_1$	$P1$
Unit-cell parameters						
a (Å)	40.86	85.61	33.20	33.08	33.18	33.11
b (Å)	48.93	85.61	41.65	41.61	68.25	41.20
c (Å)	44.61	103.98	68.76	69.04	38.71	68.81
α (°)	90.00	90.00	81.17	81.00	90.00	80.81
β (°)	93.61	90.00	89.96	90.01	108.46	89.95
γ (°)	90.00	90.00	71.46	71.14	90.00	71.08
Resolution (Å)	50.0–1.22 (1.26–1.22)	33.05–2.30 (2.38–2.30)	50.00–1.06 (1.10–1.06)	19.62–1.30 (1.35–1.30)	50.00–1.42 (1.47–1.42)	50.00–1.70 (1.73–1.70)
No. of unique reflections	50676	32781	141658	75840	30308	34187
Completeness (%)	96.8 (91.5)	99.7 (99.6)	90.3 (71.5)	90.0 (68.4)	98.3 (99.9)	91.2 (60.4)
Multiplicity	3.6 (2.9)	14.0 (11.5)	3.6 (2.5)	2.8 (2.2)	3.1 (3.0)	7.9 (7.5)
R_{merge} (%)	3.5 (39.6)	11.8 (50.5)	8.1 (36.6)	7.6 (32.5)	4.7 (31.1)	7.2 (34.6)
$\langle I/\sigma(I)\rangle$	33.6 (2.3)	15.6 (2.7)	23.6 (2.3)	13.2 (3.4)	27.9 (3.4)	12.71 (2.8)
R_{work} (%)	15.8	19.0	12.8	17.9	18.9	17.0
R_{free} (%)	18.9	24.0	15.5	22.9	21.3	20.2
R.m.s. deviations						
Bonds (Å)	0.008	0.021	0.022	0.017	0.011	0.016
Angles (°)	1.24	1.90	2.30	1.78	1.42	1.52
$\langle B$ factor$\rangle$ (Å^2)	15.5	35.9	8.5	15.0	15.9	22.9

data collected at a wavelength of 0.9780 Å showed that they belonged to space group $P4_222$ (Mn_2-Se).

2.4. Structure determination and refinement

Employing the Co^{2+} anomalous signal at a wavelength of 1.6047 Å, the Co_1 structure was solved by the single-wavelength anomalous diffraction (SAD) technique. Using *SHELX* (Sheldrick, 2008) with the *HKL2MAP* interface (Pape & Schneider, 2004), two Co^{2+} sites corresponding to the two monomers in the asymmetric unit were located, yielding an interpretable map at 1.75 Å resolution. An atomic model with one Co^{2+} ion bound in each catalytic site was built with *ARP*/*wARP* (Langer *et al.*, 2008), followed by alternating cycles of rebuilding with *Coot* (Emsley & Cowtan, 2004) and refinement with *REFMAC* (Murshudov *et al.*, 2011). This structure was used as a search model for solving the Mn_1, Mg_1-*A* and Mg_1-*B* structures, as well as the Mn_2 structure, which bound two Mn^{2+} ions, by molecular replacement using *MOLREP* (Vagin & Teplyakov, 2010). The Mn_2-Se structure was solved by Se-SAD using *SOLVE* (Terwilliger & Berendzen, 1999), which located six selenium and two Mn^{2+} sites for the two monomers in the asymmetric unit. Data-collection and refinement statistics are summarized in Table 1. Figures of protein structures were prepared using *PyMOL* (Schrödinger) and structural alignment results from the *DALI* server (Holm *et al.*, 2008) were edited manually and presented using *ESPript* (Robert & Gouet, 2014).

In the structure determination of the active centre, we confirmed the possibility of Mg^{2+} contamination, especially in Mn_1 crystals. No sign of this was detected in the refinements for metal occupancy and anomalous terms, and the Bijvoet Fourier maps show clear anomalous peaks. However, we could not fully exclude its possibility owing to experimental limitations.

2.5. Accession codes

The coordinates and structure factors have been deposited in the Protein Data Bank with accession codes 3w40 (Mg_1-*A*),

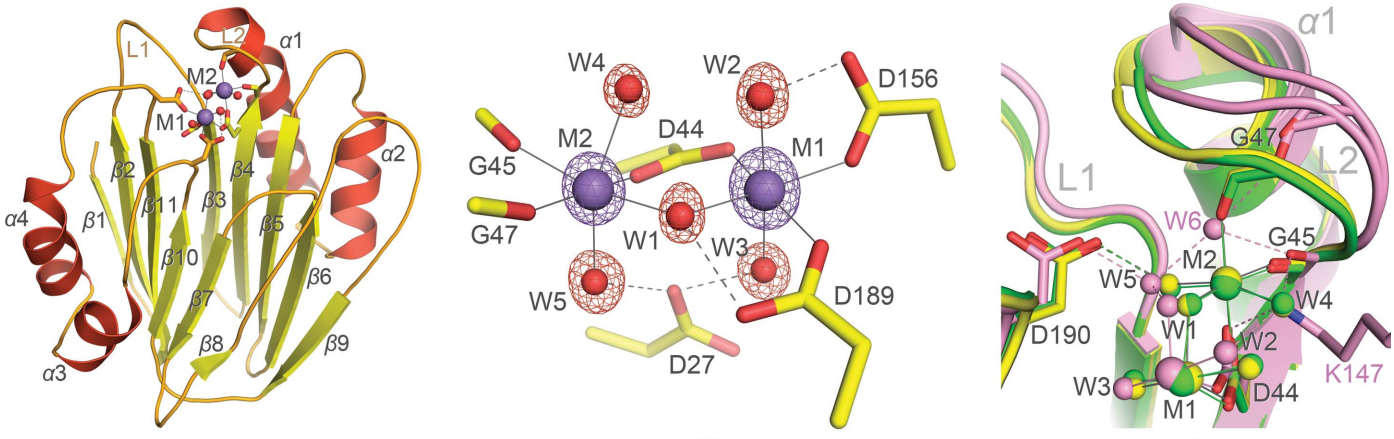

(*a*) (*b*) (*c*)

Figure 1
Crystal structure of RsbX. (*a*) Structure of Mn_2, with the two Mn^{2+} ions shown as purple spheres. (*b*) Catalytic centre of Mn_2. The $F_o - F_c$ OMIT maps for the Mn^{2+} ions (purple) and water molecules (red) are contoured at 16 and 9σ, respectively. (*c*) Superposition of the dinuclear Mn_2 (yellow), Mn_2-Se (green) and the mononuclear Mg_1-*A* (pink) structures. A substantial movement of loop L2, which contains the M2-coordinating Gly47, results in the loss of the M2 ion in Mg_1-*A*.

3w41 (Mg_1-*B*), 3w42 (Mn_1), 3w43 (Mn_2), 3w44 (Mn_2-Se) and 3w45 (Co_1).

3. Results

3.1. Overall structure

The structure of RsbX maintains the typical $\alpha\beta\beta\alpha$ sandwich fold of PPM phosphatases, with two antiparallel β-sheets flanked by two pairs of α-helices on either side (Fig. 1*a*). RsbX has 11 β-strands, and β8 is shortened because of the presence of several aromatic and proline residues (Phe122, Tyr123, Pro124 and Pro126) that reduce the hydrogen-bonding potential with β7. The catalytic centre is located at one end of the β-sandwich and is close to the β2–β3 loop, designated loop L1. Both the Mn_2 and Mn_2-Se structures bind two Mn^{2+} ions in the catalytic centre, whereas the other four structures (Mg_1-*A*, Mg_1-*B*, Mn_1 and Co_1) bind only one metal ion. The asymmetric unit of the Mn_2 structure solved in space group $P2_1$ contains one molecule, while two molecules related by twofold symmetry are present in the Mn_2-Se structure in space group $P4_222$. The three structures that belong to the same space group $P1$, Mn_1, Mg_1-*A* and Co_1, each also contains two molecules related by 2_1 symmetry in the asymmetric unit. Repeated annealing shifted the noncrystallographic 2_1 axis to a crystallographic axis, yielding the Mg_1-*B* structure in space group $P2_1$, differing from that of Mn_2. It also contains two molecules in the asymmetric unit that each bind only one metal ion.

3.2. Catalytic centre

The first Mn^{2+}-binding site in the catalytic centre of the Mn_2 structure, M1, is coordinated by Asp44, Asp156, Asp189 and three water molecules, W1–W3 (Fig. 1*b*). Asp44 and W1 also coordinate the second Mn^{2+}-binding site, M2, which is further coordinated by the backbone O atoms of Gly45 and Gly47, as well as two other water molecules, W4 and W5. W1 also binds to Asp189 and W2 to Asp156, whereas W3 and W5 both form a hydrogen bond to Asp27. In the mononuclear structures where M2 is absent, a shift of Leu46–Leu51 which also encompasses the β4–α1 loop, designated L2, away from the catalytic centre is observed, displacing the backbone O atom of Gly47 from its M2-coordinating site to allow a water molecule, W6, to bind there instead (Fig. 1*c*). There is sufficient space for Lys147 from an adjacent subunit to protrude into the catalytic centre and bind at the W4 site. An alternative conformation with a larger shift at Gly47–Ser50 is also present in Mg_1-*A* and Mn_1, while only the second conformation is present in Mg_1-*B* and Co_1. In the Mn_2-Se structure, where M2 is present, loop L2 still maintains the Gly47–M2 coordination but the region beyond this deviates into the mononuclear conformation.

Table 2
Metal bond lengths (Å) and δ_{oct} (°).

The monomers in an asymmetric unit are indicated in parentheses.

(*a*) M1.

	Asp44	Asp156	Asp189	W1	W2	W3	Average	δ_{oct}
Mn_2	2.18	2.13	2.25	2.20	2.24	2.18	2.20	7.9
Mn_2-Se (*A*)	2.36	2.12	2.36	2.29	2.35	2.29	2.29	11.8
Mn_2-Se (*B*)	2.23	2.15	2.16	2.18	2.39	2.28	2.23	8.3
Mn_1 (*A*)	2.09	2.03	2.11	2.06	2.13	2.06	2.08	4.8
Mn_1 (*B*)	2.07	2.03	2.16	2.08	2.12	2.06	2.08	4.7
Mg_1-*A* (*A*)	2.12	2.01	2.08	2.08	2.14	2.07	2.08	4.4
Mg_1-*A* (*B*)	2.10	2.01	2.06	2.09	2.14	2.03	2.07	4.1
Mg_1-*B*	2.10	2.07	2.15	2.10	2.08	2.10	2.10	4.4
Co_1 (*A*)	2.10	2.02	2.17	2.20	2.17	2.02	2.11	4.9
Co_1 (*B*)	2.11	2.18	2.22	2.05	2.19	2.02	2.13	4.9

(*b*) M2.

	Asp44	Gly45	Gly47	W1	W4	W5	Average	δ_{oct}
Mn_2	2.12	2.25	2.23	2.16	2.23	2.31	2.21	9.5
Mn_2-Se (*A*)	2.19	2.15	2.24	2.04	2.26	2.30	2.20	8.6
Mn_2-Se (*B*)	2.06	2.25	2.08	2.17	2.25	2.51	2.22	10.4

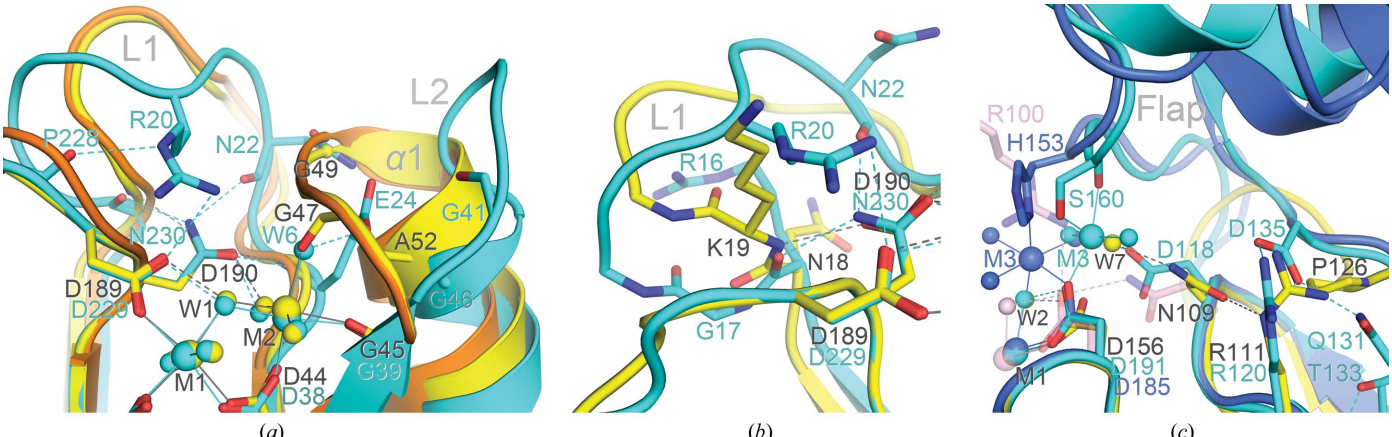

(*a*) (*b*) (*c*)

Figure 2
Structural comparison of PPM phosphatases. (*a*) Reorganization of the PPM II catalytic centre. Loops L2 of the PPM II phosphatases RsbX (yellow) and MtX (orange) tilt towards their catalytic centres and coordinate M2, whereas loop L1 of the PPM I phosphatase PstP (cyan) is anchored to its catalytic centre. (*b*) Conformation of PPM I loop L1. The strictly conserved Gly17 of PstP enables the backbone O of Arg16 to flip 180° relative to that of Asn18 in RsbX, creating room for loop L1 to fold towards the catalytic centre. (*c*) PPM I flap subdomain. The flaps of both PstP and MspP (blue) bind M3 but at different sites. Asn109 in RsbX binds water molecule W7 at the PstP M3 site, which is dislodged in the mononuclear Mg_1-*A* structure (pink).

Table 3
Kinetic parameters for RsbX acting on *p*NPP.

(*a*) Specific activity on *p*NPP with Mn^{2+}.

k_{cat} (s^{-1})	$K_m^{(pNPP)}$ (m*M*)	$k_{cat}/K_m^{(pNPP)}$ (M^{-1} s^{-1})	$K_m^{(Mn)}$ (m*M*)
0.276 ± 0.050	1.16 ± 0.42	238 ± 39	1.43 ± 0.25

(*b*) Relative activity with different metals.

Mn^{2+}	Co^{2+}	Ni^{2+}	Cu^{2+}	Zn^{2+}	Mg^{2+}
1.0	0.16	N.D.	0.08	N.D.	N.D.

In both the Mn_2 and Mn_2-Se structures with bound M1 and M2, the average bond lengths for M1 and M2 are 2.2–2.3 Å, and the r.m.s. deviations of the angles from those in ideal octahedral geometry, δ_{oct} (Harding, 2000), are 8–12° (Table 2). When compared with the four mononuclear structures (Mg_1-*A*, Mg_1-*B*, Mn_1 and Co_1) in which only M1 is bound, however, the average M1 bond lengths decrease to 2.1 Å and the δ_{oct} values fall below 5°. Mn^{2+} was required by RsbX to dephosphorylate *p*NPP, with a K_m of 1.2 m*M* and a k_{cat} of 0.28 s^{-1}, while no activity was detected when Mn^{2+} was replaced by Mg^{2+} even up to 100 m*M* (Table 3). Substitution with Co^{2+} or Cu^{2+}, meanwhile, greatly reduced the RsbX activity, and Zn^{2+} completely inactivated the phosphatase.

3.3. Comparison with PPM phosphatases

A structural similarity search using the *DALI* server (Holm *et al.*, 2008) yielded PPM phosphatases from both subfamilies I and II. The closest structure is the PPM II phosphatase MtX, which shares an identity of 24% with RsbX (Quin *et al.*, 2012), with a *Z*-score of 26.5 and an r.m.s.d. of 2.1 Å. Other PPM II structures include the phosphatase domain of Rv1364c (*Z*-score = 21.5, r.m.s.d. = 2.4 Å, 19% identity; King-Scott *et al.*, 2011), which is also highly similar, and SpoIIE (*Z*-score = 9.0, r.m.s.d. = 3.2 Å, 13% identity; Levdikov *et al.*, 2012) with a lower similarity. From the PPM I phosphatases, PstP from *M. tuberculosis* (*Z*-score = 22.4, r.m.s.d. = 2.3 Å, 19% identity; Pullen *et al.*, 2004), tPphA from the cyanobacterium *Thermosynechococcus elongatus* (*Z*-score = 21.2, r.m.s.d. = 2.4 Å, 18% identity; Schlicker *et al.*, 2008), MspP (*Z*-score = 20.0, r.m.s.d. = 2.9 Å, 14% identity; Bellinzoni *et al.*, 2007) and human PP2Cα (*Z*-score = 18.4, r.m.s.d. = 2.7 Å, 13% identity; Das *et al.*, 1996) are all closely similar.

A major difference between the PPM I and II phosphatases is observed in the M2-binding site. The N-terminus of α1 of RsbX is approximately a turn longer than those of the PPM I phosphatases, with the M2-coordinating loop L2 tilting towards the catalytic centre and loop L1 swinging away (Fig. 2*a*). Both MtX and Rv1364c also share this highly conserved M2-binding site. Loop L2 in PPM I phosphatases such as PstP, in contrast, swings away from the catalytic centre, while loop L1 is anchored to it through the highly conserved Arg20 and Asn230 (Fig. 2*a*). The ψ torsion angle of Arg16 in PstP also rotates about 180° relative to that of Asn18 in RsbX so that loop L1 can bind to the catalytic centre, but such a conformation is blocked by Lys19 in RsbX (Fig. 2*b*). The corresponding glycine in PstP, Gly41, neither coordinates any metal ion nor superposes structurally with the M2-coordinating Gly47 of RsbX. Instead, M2 is coordinated by the water molecule W6, which also binds to Glu24 in PstP, which is a well conserved Glu/Gln residue (Fig. 3). In an MspP structure, the arginine corresponding to Arg20 in PstP, Arg17, further coordinates a phosphate ion bound in the catalytic site (Bellinzoni *et al.*, 2007). Superposing this phosphate ion onto RsbX places three of the four phosphate O atoms into the W1, W2 and W4 sites, but the fourth O atom, coordinated by Arg17 in MspP, is uncoordinated.

RsbX also totally lacks the flap subdomain present in all of the PPM I structures, and this region is greatly reduced to a loop that connects β8 and β9 (Fig. 3). In PstP, Ser160 from the flap as well as the conserved Asp118 and Asp191 coordinate a third metal, M3 (Fig. 2*c*). Asp191 is strictly conserved in all PPM phosphatases, *i.e.* Asp156 in RsbX, which also coordinates M1 and W2. In RsbX, a water molecule, W7, is observed binding at the corresponding M3 site, hydrogen-bonded by Asp156 and Asn109 (Fig. 2*c*). In the four mononuclear structures of RsbX without a bound M2, Arg100 from a neighbouring monomer dislodges W7 from its site and binds to Asp156, with Asn109 also turning to bind Asp156.

4. Discussion

Despite sharing only 11–24% sequence identity, RsbX shows a high degree of structural similarity to both PPM I and PPM II phosphatases. The β-stranded core is well maintained, albeit with a greatly shortened β8, and the residues constituting the catalytic centre, including those coordinating the two Mn^{2+} ions, are highly conserved. RsbX contains an additional β1 which is absent in MtX and most of the bacterial PPM phosphatases (Fig. 3). This β1 is present in the PPM II domain of Rv1364c as a loop that interacts with its C-terminal kinase domain (King-Scott *et al.*, 2011) and in human PP2Cα, a well characterized PPM I phosphatase (Takekawa *et al.*, 1998). β1 does not seem to be involved in substrate binding, as it is shielded from the catalytic centre, and instead may be a remnant from related multidomain phosphatases such as RsbU and RsbP, in which it connects the phosphatase domain to the other domains. The RsbX structure also displays features characteristic of the PPM II phosphatases, whereas many residues critical for the formation of PPM I phosphatases are not conserved in the RsbX structure.

4.1. Metal coordination

Only M1 is observed in the mononuclear Mg_1-*A* structure, indicating that RsbX may have a very low affinity for Mg^{2+}. In the Mn_1 and Co_1 crystals, Mg^{2+} was replaced by Mn^{2+} or Co^{2+} despite being present at a fivefold higher concentration. In fact, RsbX activated with 0.1 m*M* Mn^{2+} was not inhibited by Mg^{2+} even at the 1000-fold higher concentration of 100 m*M*. The absence of M2 has caused the M2-coordinating loop L2 to shift away from the catalytic centre (Fig. 1*c*), forming a

hydrogen-bond network with a neighbouring asymmetric unit. Similar conformational shifts were observed in both the Mn_1 and Co_1 structures, most likely because their crystals were derived from Mg_1-*A* seeds. Indeed, no crystals were formed without seeding when Mg^{2+} was substituted with the other two metals under the same crystallization conditions, suggesting that with these metals RsbX was unable to form an enzyme coordinating only M1. The protein molecules hence could not pack into similar *P*1 crystals as Mg_1-*A*, in which Lys147 from a neighbouring monomer extended to bind at the W4 site (Fig. 1*c*). The Mn_2 and Mn_2-Se crystals with two bound Mn^{2+} ions, on the other hand, were formed independently under different conditions.

The formation of a dinuclear catalytic centre in RsbX results in larger distortions in the coordination of the two metal ions. Compared with the mononuclear structures that bind only M1, when M2 is also present, as in the dinuclear Mn_2 and Mn_2-Se structures, the average metal bond lengths increase by about 0.1 Å and the bond angles also undergo greater distortions from the ideal octahedral geometry, with higher δ_{oct} values (Table 2). In the mononuclear Mg_1-*A* structure the loss of the M2–Gly47 interaction results in the shift in loop L2 away from the catalytic centre (Fig. 1*c*). The flexibility of this region probably plays a role in the specificity for Mn^{2+}, which has relaxed coordination requirements compared with Mg^{2+} (Yang *et al.*, 2006).

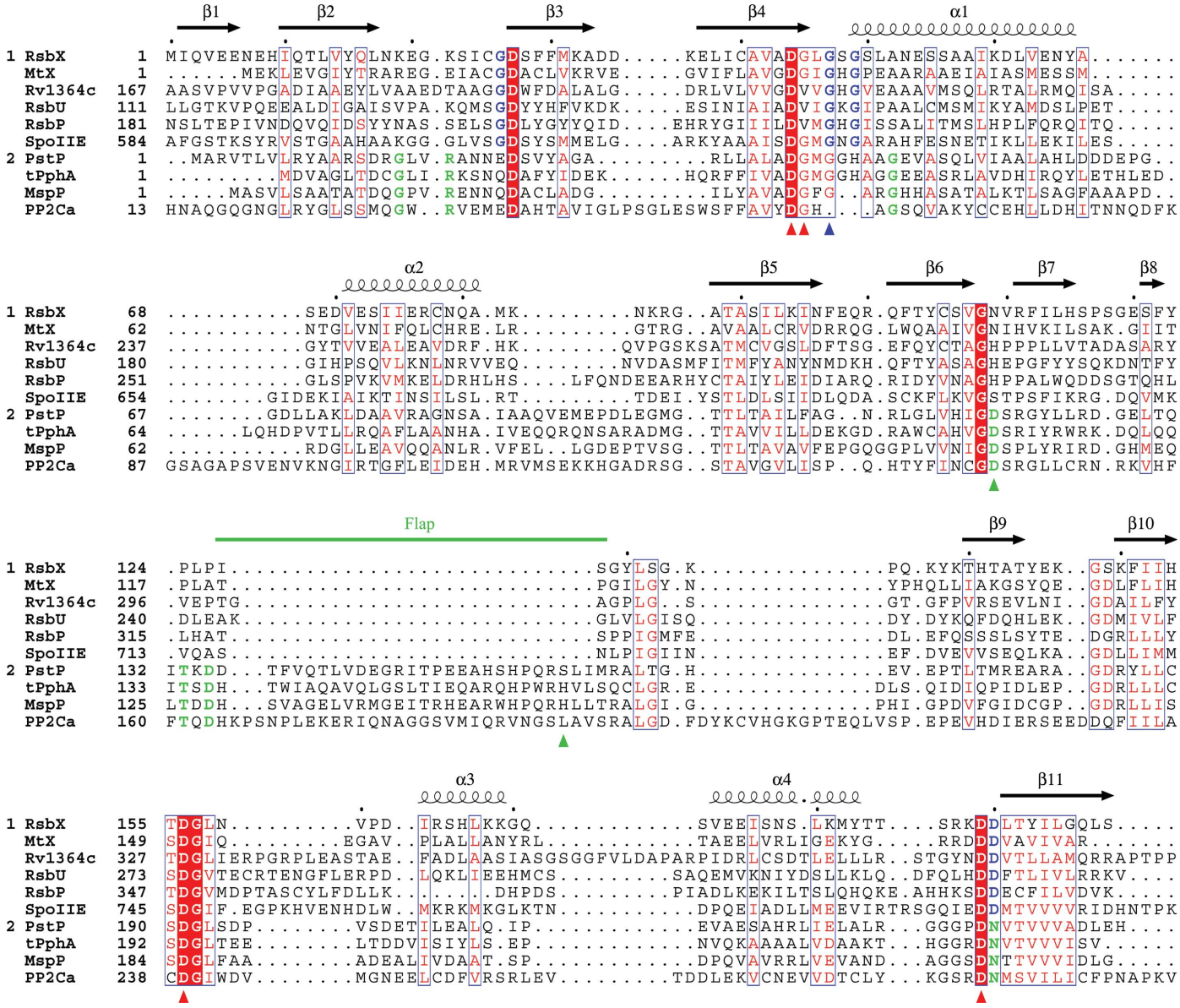

Figure 3
Sequence comparison of PPM phosphatases. The secondary structures of RsbX as well as the flap subdomain are shown above the sequences. Residues coordinating both M1 and M2 in all phosphatases are indicated by red triangles, the M2-coordinating glycine in PPM II phosphatases (group 1) by a blue triangle and M3 in some PPM I phosphatases (group 2) by green triangles. Conserved residues contributing to the catalytic centre conformation in PPM II or PPM I phosphatases are highlighted in blue or green. All phosphatases are aligned structurally except for RsbU and RsbP.

4.2. Reorganization of the catalytic centre

A defining feature of PPM II phosphatases is the coordination of M2 directly by a glycine from loop L2, instead of W6 as in PPM I phosphatases (Fig. 2*a*). This is achieved by tilting loop L2 of PPM II phosphatases towards, and tilting loop L1 away from, the catalytic centre, and the key changes for such reorganization are mostly strictly conserved and easily recognizable. Firstly, the coordination of M2 through W6 is not maintained in PPM II phosphatases. W6 is hydrogen-bonded by the side chain of a conserved Glu/Gln, *i.e.* Glu24 in PstP and Glu37 in PP2Cα, but this residue is replaced by Gly26 in RsbX, which cannot bind W6, and is strictly conserved in PPM II phosphatases (Fig. 3). Secondly, interactions that anchor loop L1 towards the catalytic centre in PPM I phosphatases, such as those of the well conserved Arg20 and Asn230 in PstP (Fig. 2*a* and 2*b*), are also no longer conserved. The corresponding Arg17 in MspP further binds a phosphate ion in the catalytic centre, thus acting as a substrate-binding residue (Bellinzoni *et al.*, 2007). The hydrogen bonding between the side chain of Asn230 in PstP and the two backbone O atoms from loop L1, meanwhile, is abolished in RsbX by replacing Asn230 with the invariant Asp190 (Fig. 2*b*).

Thirdly, substitution with smaller residues such as Gly26 and Gly49 in RsbX, both of which are strictly conserved in PPM II phosphatases, also helps to accommodate the tilting of loop L2 by reducing steric clashes. The strictly conserved Gly17 and Gly46 of PstP, on the other hand, are not conserved in PPM II phosphatases, and instead are replaced by the larger Lys19 and Ala52 in RsbX. The side chain of Lys19 in RsbX prevents loop L1 from binding to the catalytic centre, but in PstP the corresponding Gly17 enables the backbone O atom of the preceding Arg16 to flip 180° to bind to the side chain of Asn230, creating space for loop L1 to fold towards the catalytic centre (Fig. 2*b*). Ala52 of RsbX, meanwhile, pushes loop L2 towards the catalytic centre. Loop L1 of RsbX hence swings outwards to make room for the formation of the additional turn of α1 and the tilting of loop L2. These signature changes are also observed in the MtX and Rv1364c structures, as well as being present in the sequences of the phosphatase domains of RsbU and RsbP, which should also coordinate M2 likewise *via* a glycine residue from loop L2.

4.3. RsbX activity

Mn^{2+} is specifically required by RsbX and other PPM II phosphatases to dephosphorylate *p*NPP (King-Scott *et al.*, 2011; Quin *et al.*, 2012), and also by RsbX, MtX and SpoIIE to act on their respective substrate proteins RsbS-P (Yang *et al.*, 1996), MtS-P (Quin *et al.*, 2012) and SpoIIAA-P (Levdikov *et al.*, 2012). Human PP2Cα, on the other hand, requires Mn^{2+} for the dephosphorylation of *p*NPP but requires Mg^{2+} bound to a low-affinity M3 site for a phosphopeptide substrate (Tanoue *et al.*, 2013; Marley *et al.*, 1996). tPphA also requires M3 to provide a water molecule as a proton donor during catalysis (Su *et al.*, 2011). With the observation of occupancy at the RsbX M2 site in only Mn_2 but not Mn_1, its low binding affinity may be owing to the flexibility of the loop L2 region, which in the absence of M2 swings away from the M2-binding site (Fig. 1*c*). This flexibility may play a role in Mn^{2+} specificity, which can be further regulated by Mn^{2+} levels. It has also been suggested that low levels of Mn^{2+} could activate σ^B by stimulating the phosphatase activity of RsbU (Guedon *et al.*, 2003), which is expected to share a similar catalytic centre as RsbX owing to their sequence similarity.

RsbX acts specifically on the phosphorylated Ser59 of RsbS and Thr205 of RsbR. From a model based on the stressosome structures (Marles-Wright *et al.*, 2008), these two well conserved residues are located on the surfaces of the STAS domains (Supplementary Fig. S1). Ser59 in RsbS is well positioned to interact directly with RsbX, whereas Thr205 in RsbR, which is situated close to the groove between the N-terminal domain and the STAS domain of RsbR, may be less readily accessible to RsbX. Thr171 in RsbR, on the other hand, is located in the groove, which appears to be even more difficult for RsbX to access (Supplementary Fig. S1), in accordance with the reported lack of RsbX activity towards Thr171 of RsbR (Chen *et al.*, 2004). Thr171 of RsbR is phosphorylated in unstressed cells (Eymann *et al.*, 2011), and the N-terminal domain of RsbR may have prevented RsbX from approaching and dephosphorylating it. Ser59 of RsbS may also be phosphorylated in unstressed cells, but RsbX can immediately dephosphorylate it for the stressosome to recapture RsbT. In the presence of stress, however, this balance is tilted towards the kinase activity of RsbT by an as-yet unknown mechanism, enabling RsbT to phosphorylate Ser59 of RsbS and Thr205 of RsbR efficiently so as to activate σ^B. The mechanism of the stressosome-mediated signalling is still far from being completely understood, not least because the signalling molecule that interacts with the stressosome and triggers the whole stress response pathway has yet to be identified.

Acknowledgements

This work was supported in part by MEXT/JSPS KAKENHI (17770085, 19570102, 22770142, 23121537 and 25121746). We would like to thank Tetsuya Shimizu and Tomonori Kaneko for invaluable discussions. The experiments were conducted on beamlines BL41XU (Proposal No. 2007B1348) and BL38B1 (2008A1233) at SPring-8, beamlines BL26B1/B2 at RIKEN (20080109) and at the Photon Factory (2006G147).

References

Bellinzoni, M., Wehenkel, A., Shepard, W. & Alzari, P. M. (2007). *Structure*, **15**, 863–872.
Benson, A. K. & Haldenwang, W. G. (1992). *J. Bacteriol.* **174**, 749–757.
Bork, P., Brown, N. P., Hegyi, H. & Schultz, J. (1996). *Protein Sci.* **5**, 1421–1425.
Brody, M. S., Vijay, K. & Price, C. W. (2001). *J. Bacteriol.* **183**, 6422–6428.
Chen, C.-C., Lewis, R. J., Harris, R., Yudkin, M. D. & Delumeau, O. (2003). *Mol. Microbiol.* **49**, 1657–1669.
Chen, C.-C., Yudkin, M. D. & Delumeau, O. (2004). *J. Bacteriol.* **186**, 6830–6836.

Das, A. K., Helps, N. R., Cohen, P. T. & Barford, D. (1996). *EMBO J.* **15**, 6798–6809.
Delumeau, O., Lewis, R. J. & Yudkin, M. D. (2002). *J. Bacteriol.* **184**, 5583–5589.
Dufour, A. & Haldenwang, W. G. (1994). *J. Bacteriol.* **176**, 1813–1820.
Dufour, A., Voelker, U., Voelker, A. & Haldenwang, W. G. (1996). *J. Bacteriol.* **178**, 3701–3709.
Duncan, L., Alper, S., Arigoni, F., Losick, R. & Stragier, P. (1995). *Science*, **270**, 641–644.
Emsley, P. & Cowtan, K. (2004). *Acta Cryst.* D**60**, 2126–2132.
Eymann, C., Schulz, S., Gronau, K., Becher, D., Hecker, M. & Price, C. W. (2011). *Mol. Microbiol.* **80**, 798–810.
Guedon, E., Moore, C. M., Que, Q., Wang, T., Ye, R. W. & Helmann, J. D. (2003). *Mol. Microbiol.* **49**, 1477–1491.
Haldenwang, W. G. (1995). *Microbiol. Rev.* **59**, 1–30.
Harding, M. M. (2000). *Acta Cryst.* D**56**, 857–867.
Hecker, M. & Völker, U. (1998). *Mol. Microbiol.* **29**, 1129–1136.
Holm, L., Kääriäinen, S., Rosenström, P. & Schenkel, A. (2008). *Bioinformatics*, **24**, 2780–2781.
Igo, M., Lampe, M., Ray, C., Schafer, W., Moran, C. P. Jr & Losick, R. (1987). *J. Bacteriol.* **169**, 3464–3469.
Kim, T.-J., Gaidenko, T. A. & Price, C. W. (2004). *J. Mol. Biol.* **341**, 135–150.
King-Scott, J., Konarev, P. V., Panjikar, S., Jordanova, R., Svergun, D. I. & Tucker, P. A. (2011). *Structure*, **19**, 56–69.
Langer, G., Cohen, S. X., Lamzin, V. S. & Perrakis, A. (2008). *Nature Protoc.* **3**, 1171–1179.
Levdikov, V. M., Blagova, E. V., Rawlings, A. E., Jameson, K., Tunaley, J., Hart, D. J., Barak, I. & Wilkinson, A. J. (2012). *J. Mol. Biol.* **415**, 343–358.
Marles-Wright, J., Grant, T., Delumeau, O., van Duinen, G., Firbank, S. J., Lewis, P. J., Murray, J. W., Newman, J. A., Quin, M. B., Race, P. R., Rohou, A., Tichelaar, W., van Heel, M. & Lewis, R. J. (2008). *Science*, **322**, 92–96.
Marley, A. E., Sullivan, J. E., Carling, D., Abbott, W. M., Smith, G. J., Taylor, I. W., Carey, F. & Beri, R. K. (1996). *Biochem. J.* **320**, 801–806.
Murshudov, G. N., Skubák, P., Lebedev, A. A., Pannu, N. S., Steiner, R. A., Nicholls, R. A., Winn, M. D., Long, F. & Vagin, A. A. (2011). *Acta Cryst.* D**67**, 355–367.
Otwinowski, Z. & Minor, W. (1997). *Methods Enzymol.* **276**, 307–326.
Pape, T. & Schneider, T. R. (2004). *J. Appl. Cryst.* **37**, 843–844.
Price, C. W., Fawcett, P., Cérémonie, H., Su, N., Murphy, C. K. & Youngman, P. (2001). *Mol. Microbiol.* **41**, 757–774.
Pullen, K. E., Ng, H.-L., Sung, P.-Y., Good, M. C., Smith, S. M. & Alber, T. (2004). *Structure*, **12**, 1947–1954.
Quin, M. B., Berrisford, J. M., Newman, J. A., Baslé, A., Lewis, R. J. & Marles-Wright, J. (2012). *Structure*, **20**, 350–363.
Rantanen, M. K., Lehtiö, L., Rajagopal, L., Rubens, C. E. & Goldman, A. (2007). *FEBS J.* **274**, 3128–3137.
Robert, X. & Gouet, P. (2014). *Nucleic Acids Res.* **42**, W320–W324.
Schlicker, C., Fokina, O., Kloft, N., Grüne, T., Becker, S., Sheldrick, G. M. & Forchhammer, K. (2008). *J. Mol. Biol.* **376**, 570–581.
Sheldrick, G. M. (2008). *Acta Cryst.* A**64**, 112–122.
Shi, L. (2004). *Front. Biosci.* **9**, 1382–1397.
Su, J., Schlicker, C. & Forchhammer, K. (2011). *J. Biol. Chem.* **286**, 13481–13488.
Suganuma, M., Teh, A. H., Makino, M., Shimizu, N., Kaneko, T., Hirata, K., Yamamoto, M. & Kumasaka, T. (2009). *Acta Cryst.* F**65**, 1128–1130.
Takekawa, M., Maeda, T. & Saito, H. (1998). *EMBO J.* **17**, 4744–4752.
Tanoue, K., Miller Jenkins, L. M., Durell, S. R., Debnath, S., Sakai, H., Tagad, H. D., Ishida, K., Appella, E. & Mazur, S. J. (2013). *Biochemistry*, **52**, 5830–5843.
Terwilliger, T. C. & Berendzen, J. (1999). *Acta Cryst.* D**55**, 849–861.
Vagin, A. & Teplyakov, A. (2010). *Acta Cryst.* D**66**, 22–25.
Vijay, K., Brody, M. S., Fredlund, E. & Price, C. W. (2000). *Mol. Microbiol.* **35**, 180–188.
Wehenkel, A., Bellinzoni, M., Schaeffer, F., Villarino, A. & Alzari, P. M. (2007). *J. Mol. Biol.* **374**, 890–898.
Yang, X., Kang, C. M., Brody, M. S. & Price, C. W. (1996). *Genes Dev.* **10**, 2265–2275.
Yang, W., Lee, J. Y. & Nowotny, M. (2006). *Mol. Cell*, **22**, 5–13.